MRS Advances © 2020 The Author(s), corrected publication 2022
DOI: 10.1557/adv.2020.312

Elucidating the evolution of silicon anodes in lithium based batteries

Wenzao Li,[1,†] Mallory N. Vila,[1,†] Esther S. Takeuchi,[1,2,3] Kenneth J. Takeuchi,[1,2] Amy C. Marschilok[1,2,3,*]

[1]*Department of Chemistry, Stony Brook University, Stony Brook, NY 11794*

[2]*Department of Materials Science and Chemical Engineering, Stony Brook University, Stony Brook, NY 11794*

[3]*Energy and Photon Sciences Directorate, Brookhaven National Laboratory, Upton NY 11973*

† equal contributions by W. Li and M. Vila.

**Corresponding author: amy.marschilok@stonybrook.edu*

Silicon has attracted particular attention as a potential high capacity material for lithium based batteries. However, the application of Si-based electrodes remains challenging, in major part due to its significant irreversible energy loss during cycling. Here isothermal microcalorimetry (IMC) is demonstrated to be a precise and operando characterization method for tracking a battery's thermal behaviour and deconvoluting the contributions from electrochemical polarization, entropy change, and parasitic reactions. Cyclic voltammetry (CV), electrochemical impedance spectroscopy (EIS), and x-ray powder diffraction (XRD) further elucidate the Si reactivity in conjunction with the IMC.

INTRODUCTION

Lithium ion batteries (LIBs) have shown significant success under application for consumer electronics. Nevertheless, non-negligible heat generation can reduces the useful energy density, poses a potential safety hazard and shortens battery life-time.[1, 2] To avoid possible risks, advanced characterization methods should be utilized to gain a comprehensive understanding of a battery's thermal behaviour to help mitigate unnecessary heat propagation and the associated parasitic reactions.

Calorimetry through cell and component level studies has been shown to be a powerful approach to assess safety of lithium ion battery systems.[3, 4] Isothermal microcalorimetry (IMC) has also been employed as a tool to characterize the evolution of multiple battery systems, including Li/graphite,[5] Li/Fe_3O_4,[6, 7] Li/$LiNi_{0.8}Mn_{0.1}Co_{0.1}O_2$(NMC811),[8] graphite/$LiCoO_2$,[9] and Li/$Li_2Ru_{0.75}Sn_{0.25}O_3$.[10] The heat flow (instantaneous power) monitored by the IMC can be further analysed by a 3-component model where the total heat flow is composed of polarization, entropic heat, and parasitic reaction heat.[11] Determining the magnitude of the heat flow specifically attributable to parasitic reactions can help diagnose battery failure and provide insight on the mechanisms that contribute to limited cyclability.[12]

Among various electrode materials for LIBs, silicon has attracted particular attention, as it can achieve an ultrahigh theoretical electrochemical capacity (3579 mAh/g), when reaching a lithium-rich state ($Li_{15}Si_4$).[13, 14] However, the application of Si-based electrodes remains challenging, primarily due to its poor cyclability, which is commonly attributed to a substantial volume change of the Si particles and irreversible electrode-electrolyte side reactions, including the continuous and repetitive formation of solid-electrolyte interphase (SEI).[15, 16] The cyclability of the electrode will be impaired if deposition of the electrolyte's decomposition products continues (if additional SEI continues to form) throughout extended cycling.[17] This thickening will lead to high internal resistance, low Coulombic efficiency (CE), and decreased reversible capacity.[17, 18] As Si experiences a substantial volume increase upon lithiation, the SEI layer cracks and exposes fresh Si, therefore understanding the particular state of lithiation at which this process occurs is valuable.[19, 20]

Herein, we illustrate a general approach to monitoring heat generated from a cycling battery with IMC. A model battery system with Si-based cathode and lithium metal anode serves as an example to illustrate that *operando* IMC characterization is an insightful supplement to conventional battery testing protocols for understanding electrochemical behaviour and diagnosing battery failure mechanisms. Since conductive carbon can serve as a heat flow source by participating in (de)lithiation and contributing to electrolyte decomposition reactions, carbon was deliberately excluded from these electrodes. To further understand how parasitic reactions affect extended cycling and contribute to potential cell failure, X-ray diffraction (XRD) was collected after 30 cycles to resolve the phase changes in the silicon electrode and formation of crystalline SEI products.

EXPERIMENTAL METHODS

A working electrode composed of 80 wt% of silicon nano-powder and 20 wt% poly(vinylidene fluoride) (PVDF) in N-methyl-2-pyrrolidone was paired with a lithium metal anode using 1M $LiPF_6$ in ethylene carbonate (EC)/dimethyl carbonate (DMC) (3:7 v/v) as electrolyte. Coin-type cells were assembled within an argon-filled glovebox. To

capture the heat flow signal, a TA Instruments TAM III Isothermal Microcalorimeter was used. The IMC testing ampoule was emerged in oil at a constant temperature of 30°C. A BioLogic VSP potentiostat was used for all electrochemical measurements, except the thirty cycle galvanostatic measurement, where coin type cells were tested using a MACCOR series 4000 battery tester. For the two cycle experiment associated with IMC, the coin cell was (de)lithiated galvanostatically. Before and after each (de)lithiation step, a 12-hour rest was allowed to dissipate the residual heat and equilibrate the cell. For the thirty cycle experiment associated with X-ray diffraction, the coin cell was (de)lithiated galvanostatically at a current density of 0.2 mA/cm^2 under a potential range of 0.01 to 1.2 V versus Li/Li$^+$. The XRD patterns were collected using a Rigaku X-ray powder diffractometer with copper K-alpha radiation.

RESULTS AND DISCUSSION

Figure 1 exhibits an example utilizing the IMC to monitor the heat flow dissipation upon the first two cycles of (de)lithiation of a Li/Si half-type coin cell, using a consistent scale throughout to enable data comparison for (de)lithation and between cycles 1 and 2. The first lithiation reached a specific capacity of ~2500 mAh/g (corresponding to electron equivalents of 2.62) and the subsequent cycles were controlled by potential limits of 1.2 V (vs. Li/Li$^+$) for delithiation and 1 mV (vs. Li/Li$^+$) for lithiation (**Figure 2**).

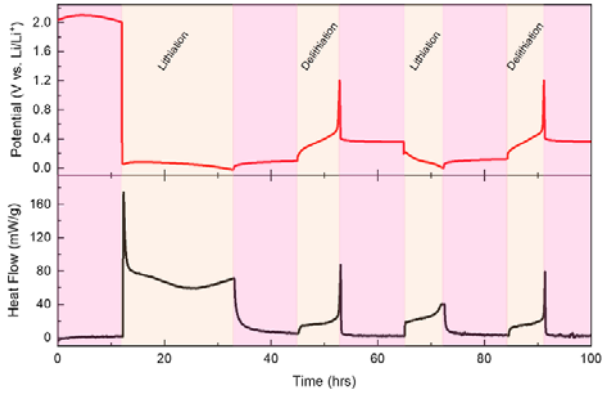

Figure 1. A Si/Li half-type coin cell (de)lithiated inside the IMC at a current density of 0.15 mA/cm^2 with 12-hr rest time intervals. The galvanostatic cycling (red) and the corresponding heat flow (black) were collected simultaneously.

During the 1st cycle lithiation, the potential decreases quickly from the open-circuit potential (OCP) (~2.0 V) to ~0.07 V and a plateau is observed at ~0.05 V (Figure 2a). This plateau indicates a two-phase reaction, in accordance with the amorphization of crystalline silicon.[21] The first lithiation delivers a capacity of 2504 mAh/g (~2.62 equiv. of Li), concomitant with a significant heat flow signal. This sharp heat flow peak (~175 mW/g) occurs almost instantly (~0.04 equiv of Li), and then gradually decreases to a diminished heat flow of ~70 mW/g. The 1st cycle delithiation extracts ~0.99 equiv of Li with a corresponding capacity of 947 mAh/g (Figure 2b). The 2nd lithiation (Figure 2c) and delithiation (Figure 2d) reach capacities of 894 mAh/g (~0.94 equiv of Li) and 818 mAh/g (~0.86 equiv of Li), respectively indicating a much higher Coulombic efficiency (CE) in the 2nd cycle (91.5%) than in the 1st cycle (37.8%).

The total heat released from the 1st cycle lithiation is disproportionally higher than the subsequent cycle (Table 1). The high thermal energy output in the 1st cycle lithiation is due to not only a higher delivered electrochemical capacity, but also contributions from entropy change and parasitic reactions.[5, 16] The significant entropy change is related to a solid-state phase change of crystalline silicon to amorphous silicon.[21-23] Meanwhile, parasitic reactions, including continuous formation of the SEI, electrolyte decompositon, and active material loss due to silicon particle fracture, also account for a large portion of the heat flow.[16] In order to further characterize the generated heat flow described above, complementary techniques were utilized to probe electrolyte decomposition and the subsequent production of the SEI.

Table 1. (De)Lithiation Total Heat Flow for Cycles 1 and 2

	1st cycle	2nd cycle
Lithiation total heat (mWh/g)	1431.7	183.9
Delithiation total heat (mWh/g)	137.3	106.3

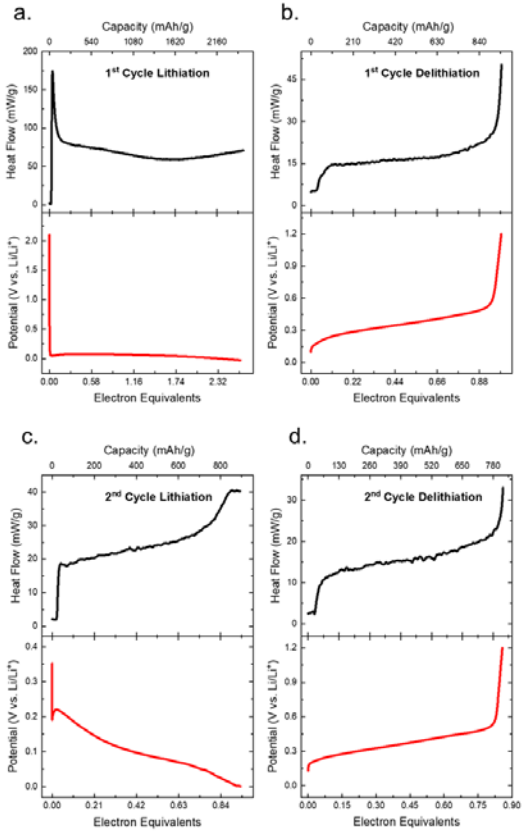

Figure 2. Heat flow (black) and galvanostatic cycling profile (red) for the (a) 1st cycle lithiation, (b) 1st cycle delithiation, (c) 2nd cycle lithiation, and (d) 2nd cycle delithiation.

Cyclic voltammetry (CV) was collected to provide insight on the chemical processes during the first two cycles of delithiation and lithiation to capture the onset of SEI formation (**Figure 3**). The two cathodic peaks suggest EC reduction and lithium alloying with silicon at 1.45 and 0.78 V, respectively, (**Figure 3, inset**).[24, 25] However, these peaks dissipate in the second cycle upon the initial formation of the SEI and the irreversible amorphization of crystalline silicon as discussed in greater detail below. In addition to quantifying the reduction potential of SEI formation, the recession of the peaks provides insight into the sluggish-alloying between the Li and Si electrodes.

Upon oxidation, the emergence of two visible peaks indicates that the dealloying process proceeds at a faster rate than alloying, which is inhibited by Si volume expansion and subsequent pulverization.[25] The anodic peaks at ~0.3 and 0.5 V are attributed to Si-Li dealloying and silicon oxide formation.[26, 27] As cycling proceeds, the 0.5 V anodic peak disappears merging into one resolved peak implying the irreversible alloying of amorphized silicon, consistent with galvanostatic cycling and heat flow profiles. The changes in current suggest an adjustment in kinetic behavior as the Li is extracted from the Si electrode, attributed to the volume changes upon expansion/contraction contributing to Si strain and stress.[26]

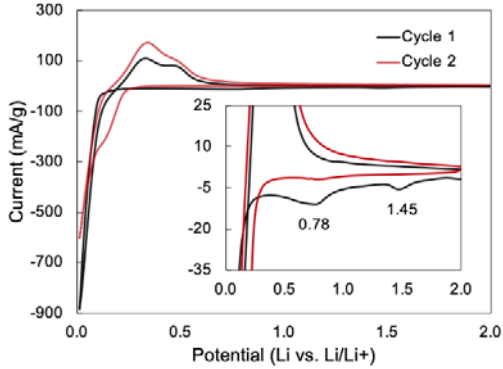

Figure 3. Cyclic voltammetry scan of three cycles from 0.1- 2 V at a scan rate of 0.1 mV/s.

Electrochemical impedance spectroscopy (EIS) was utilized to compare the electrochemical impedance of a pristine cell to that of a cycled cell (**Figure 4**). The formation of the semicircle in the cycled Si electrode at high frequencies (**Figure 4A**), in addition to the change in slope of the diffusional tail (**Figure 4B**) suggests additional SEI formation. Ideally, a robust SEI should protect against the direct active material/electrolyte continued interaction and withstand the particle expansion and contraction. However for silicon, the unstable SEI introduced by conventional electrolyte fails to act as a protective barrier, which contributes to further parasitic reaction as reflected by the heat flow.

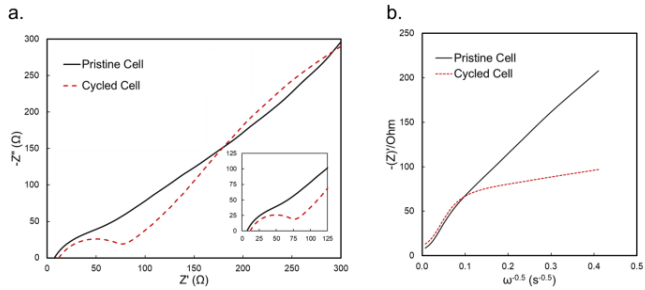

Figure 4. Comparison of the impedance data of a pristine Si electrode and a cycled Si electrode in a Nyquist plot (a) and Bode plot of the angular frequency vs Z_{real} (b).

To further understand how parasitic reactions affect extended cycling and contribute to potential cell failure, X-ray diffraction (XRD) was collected after 30 cycles. The galvanostatic cycling (**Figure 5**) exhibits significant cycle 1 irreversible capacity, consistent with the IMC data discussed above. The XRD data from the lithiated Si electrode was indexed by considering Si phases (elemental Si and $Li_{15}Si_4$) and inorganic species that might have been deposited on the electrode surface during cycling (LiF and $LiPF_6$) (**Figure 6**). The amorphous pattern at the end of the 30 cycles indicates amorphization of crystalline Si, along with emergence of crystalline $Li_{15}Si_4$.[16] The lithiated silicon electrode shows an absence of $LiPF_6$ peaks but evidence of LiF. It is proposed that LiF generated from the decomposition of $LiPF_6$ forms part of the SEI layers (**Eq. 1-3**).[28]

$$LiPF_6 \rightarrow LiF + PF_5 \quad (1)$$

$$PF_5 + H_2O \rightarrow POF_3 + 2HF \quad (2)$$

$$ROCO_2Li,\ Li_2CO_3 + HF \rightarrow LiF + ROCO_2H,\ H_2CO_3 \quad (3)$$

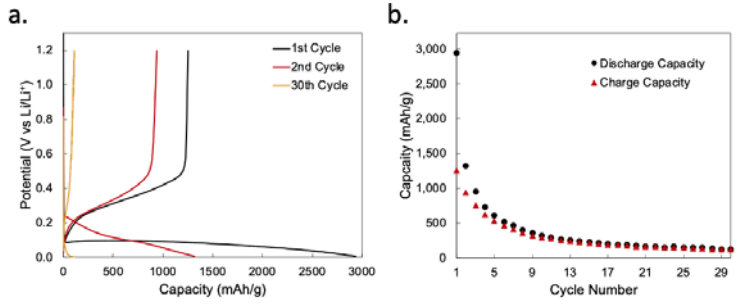

Figure 5. (a) Galvanostatic cycling of the Si/Li cell (dis)charged for 30 cycles at a current density of 0.2 mA/cm^2 and (b) the respective (dis)charge capacity displayed as a function of cycle number.

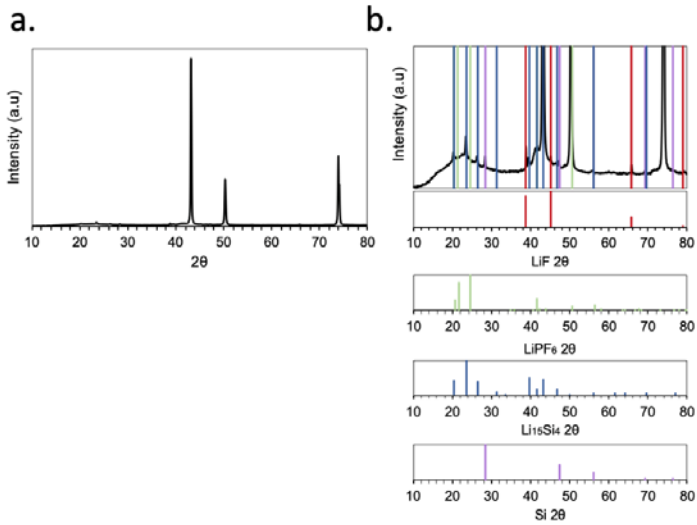

Figure 6. X-ray diffraction pattern of the lithiated Si electrode. (a) full scale, (b) scale adjusted to show indexes clearly. The unindexed peak at 75° two-theta corresponds to Cu and originates from the electrode current collector.

Due in part to its limited solubility in the carbonate-based electrolyte, LiF is proposed to create an interphase on the surface of the Si electrode which can mitigate further parasitic reactions.[29, 30] Additionally, when compared to a carbonate-based SEI layer, LiF can increase the rate of ion diffusion by preventing the growth of Li dendrites through the production of a more resistant SEI.[30] The proposed SEI formation and fracture mechanism is schematically summarized below (**Figure 7**).

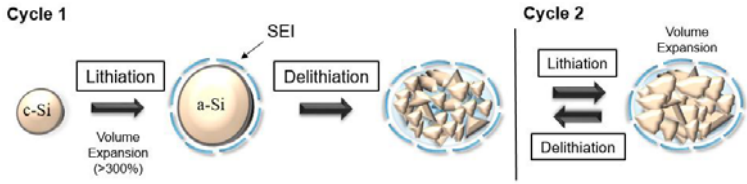

Figure 7. Schematic showing the proposed mechanism of SEI layer formation and fracturing of the Si nanoparticles throughout cycling.

SUMMARY

In this work, operando IMC was employed to capture heat flow released from a Si/Li cell during the first two cycles of galvanostatic cycling. The 1st cycle produces the most heat (1431.7 mWh/g upon lithiation and 183.9 mWh/g upon delithiation), accompanied by the largest reversible capacity loss (CE of ~38%). The significant heat associated with the 1st cycle is ascribed to substantial polarization, entropy change due to structural transformation, and parasitic reactions, including the repetitive formation of SEI.

Characterization, including CV, EIS, and XRD, were utilized to verify the underlying material evolution and surface reactions indicated by heat flow dissipation mechanism. Coupled with conventional electrochemical characterization protocols, IMC is shown to function as an insightful battery testing method, especially for conversion and alloying-type electrodes and electrode materials with a chemically active interface.

ACKNOWLEDGEMENT

The microcalorimetry of silicon work was supported by Mercedes-Benz Research and Development North America, Inc., through a gift to the Stony Brook University Foundation. The in-situ XRD and materials characterization was supported by the Center for Mesoscale Transport Properties (m2M/t), an Energy Frontier Research Center funded by the U.S. Department of Energy, Office of Science, Basic Energy Sciences, under Award #DE-SC0012673. E.S.T. acknowledges the William and Jane Knapp Chaired Professorship of Energy and the Environment.

References:

1. A. Mills and S. Al-Hallaj: Simulation of passive thermal management system for lithium-ion battery packs. *Journal of Power Sources* **141**, 307 (2005).
2. Y. Abdul-Quadir, T. Laurila, J. Karppinen, K. Jalkanen, K. Vuorilehto, L. Skogström and M. Paulasto-Kröckel: Heat generation in high power prismatic Li-ion battery cell with LiMnNiCoO2 cathode material. *International Journal of Energy Research* **38**, 1424 (2014).
3. H.M. Barkholtz, Y. Preger, S. Ivanov, J. Langendorf, L. Torres-Castro, J. Lamb, B. Chalamala and S.R. Ferreira: Multi-scale thermal stability study of commercial lithium-ion batteries as a function of cathode chemistry and state-of-charge. *Journal of Power Sources* **435**, 226777 (2019).
4. R.C. Shurtz, Y. Preger, L. Torres-Castro, J. Lamb, J.C. Hewson and S. Ferreira: Perspective—From Calorimetry Measurements to Furthering Mechanistic Understanding and Control of Thermal Abuse in Lithium-Ion Cells. *Journal of The Electrochemical Society* **166**, A2498 (2019).
5. L.J. Krause, L.D. Jensen and J.R. Dahn: Measurement of parasitic reactions in Li ion cells by electrochemical calorimetry. *Journal of The Electrochemical Society* **159**, A937 (2012).
6. M.M. Huie, D.C. Bock, A.M. Bruck, K.R. Tallman, L.M. Housel, L. Wang, J. Thieme, K.J. Takeuchi, E.S. Takeuchi and A.C. Marschilok: Isothermal Microcalorimetry: Insight into the Impact of Crystallite Size and Agglomeration on the Lithiation of Magnetite, Fe3O4. *ACS Applied Materials & Interfaces* **11**, 7074 (2019).
7. M.M. Huie, D.C. Bock, L. Wang, A.C. Marschilok, K.J. Takeuchi and E.S. Takeuchi: Lithiation of Magnetite (Fe3O4): Analysis Using Isothermal Microcalorimetry and Operando X-ray Absorption Spectroscopy. *The Journal of Physical Chemistry C* **122**, 10316 (2018).
8. J. Li, L.E. Downie, L. Ma, W. Qiu and J.R. Dahn: Study of the failure mechanisms of LiNi0. 8Mn0. 1Co0. 1O2 cathode material for lithium ion batteries. *Journal of The Electrochemical Society* **162**, A1401 (2015).
9. L.E. Downie, S.R. Hyatt, A.T.B. Wright and J.R. Dahn: Determination of the time dependent parasitic heat flow in lithium ion cells using isothermal microcalorimetry. *The Journal of Physical Chemistry C* **118**, 29533 (2014).

10. G. Assat, S.L. Glazier, C. Delacourt and J.-M. Tarascon: Probing the thermal effects of voltage hysteresis in anionic redox-based lithium-rich cathodes using isothermal calorimetry. *Nature Energy* **4**, 647 (2019).
11. L.E. Downie and J.R. Dahn: Determination of the voltage dependence of parasitic heat flow in lithium ion cells using isothermal microcalorimetry. *Journal of The Electrochemical Society* **161**, A1782 (2014).
12. L. Downie and J. Dahn: Determination of the Voltage Dependence of Parasitic Heat Flow in Lithium Ion Cells Using Isothermal Microcalorimetry. *Journal of The Electrochemical Society* **161**, 1782 (2014).
13. C. Xu, F. Lindgren, B. Philippe, M. Gorgoi, F. Björefors, K. Edström and T. Gustafsson: Improved Performance of the Silicon Anode for Li-Ion Batteries: Understanding the Surface Modification Mechanism of Fluoroethylene Carbonate as an Effective Electrolyte Additive. *Chemistry of Materials* **27**, 2591 (2015).
14. X. Zuo, J. Zhu, P. Müller-Buschbaum and Y.-J. Cheng: Silicon based lithium-ion battery anodes: A chronicle perspective review. *Nano Energy* **31**, 113 (2017).
15. X. Su, Q. Wu, J. Li, X. Xiao, A. Lott, W. Lu, B.W. Sheldon and J. Wu: Silicon-Based Nanomaterials for Lithium-Ion Batteries: A Review. *Advanced Energy Materials* **4**, 1300882 (2014).
16. L.M. Housel, W. Li, C.D. Quilty, M.N. Vila, L. Wang, C.R. Tang, D.C. Bock, Q. Wu, X. Tong, A.R. Head, K.J. Takeuchi, A.C. Marschilok and E.S. Takeuchi: Insights into Reactivity of Silicon Negative Electrodes: Analysis Using Isothermal Microcalorimetry. *ACS Applied Materials & Interfaces* **11**, 37567 (2019).
17. S. Chattopadhyay, A.L. Lipson, H.J. Karmel, J.D. Emery, T.T. Fister, P.A. Fenter, M.C. Hersam and M.J. Bedzyk: In Situ X-ray Study of the Solid Electrolyte Interphase (SEI) Formation on Graphene as a Model Li-ion Battery Anode. *Chemistry of Materials* **24**, 3038 (2012).
18. P.B. Balbuena and Y. Wang: Lithium-ion batteries: solid-electrolyte interphase, (Imperial college press2004).
19. K. Guerin: Effect of Graphite Crystal Structure on Lithium Electrochemical Intercalation. *Journal of The Electrochemical Society* **146**, 3660 (1999).
20. J.-H. Cho and S.T. Picraux: Silicon Nanowire Degradation and Stabilization during Lithium Cycling by SEI Layer Formation. *Nano Letters* **14**, 3088 (2014).
21. J. Li and J.R. Dahn: An in situ X-ray diffraction study of the reaction of Li with crystalline Si. *Journal of The Electrochemical Society* **154**, A156 (2007).
22. S. Al Hallaj, R. Venkatachalapathy, J. Prakash and J.R. Selman: Entropy changes due to structural transformation in the graphite anode and phase change of the LiCoO2 cathode. *Journal of the Electrochemical Society* **147**, 2432 (2000).
23. Y. Reynier, J. Graetz, T. Swan-Wood, P. Rez, R. Yazami and B. Fultz: Entropy of Li intercalation in Li x CoO 2. *Physical Review B* **70**, 174304 (2004).
24. J.M.M. de la Hoz and P.B. Balbuena: Reduction mechanisms of additives on Si anodes of Li-ion batteries. *Physical Chemistry Chemical Physics* **16**, 17091 (2014).
25. W.-R. Liu, Z.-Z. Guo, W.-S. Young, D.-T. Shieh, H.-C. Wu, M.-H. Yang and N.-L. Wu: Effect of electrode structure on performance of Si anode in Li-ion batteries: Si particle size and conductive additive. *Journal of Power Sources* **140**, 139 (2005).
26. L.B. Chen, J.Y. Xie, H.C. Yu and T.H. Wang: An amorphous Si thin film anode with high capacity and long cycling life for lithium ion batteries. *Journal of Applied Electrochemistry* **39**, 1157 (2009).
27. H. Shobukawa, J. Alvarado, Y. Yang and Y.S. Meng: Electrochemical performance and interfacial investigation on Si composite anode for lithium ion batteries in full cell. *Journal of Power Sources* **359**, 173 (2017).

28. T. Hou, G. Yang, N.N. Rajput, J. Self, S.-W. Park, J. Nanda and K.A. Persson: The influence of FEC on the solvation structure and reduction reaction of LiPF6/EC electrolytes and its implication for solid electrolyte interphase formation. *Nano Energy* **64**, 103881 (2019).
29. B.H. Shen, S. Wang and W.E. Tenhaeff: Ultrathin conformal polycyclosiloxane films to improve silicon cycling stability. *Science advances* **5**, eaaw4856 (2019).
30. S. Choudhury and L.A. Archer: Lithium fluoride additives for stable cycling of lithium batteries at high current densities. *Advanced Electronic Materials* **2**, 1500246 (2016).